Supporting information

Fabrication of graphene oxide/zeolitic imidazolate frameworks-8 (GO/ZIF-8) composite with enhanced adsorptive and piezo-assisted photocatalytic removal of organic dyes

Milad Atighi [a,1], Ghazaleh Falahati [a,1], Mahdi Hasanzadeh [a], Najmeh Gholami [a], Hanieh Ahmadi [a], Mina Najafi [b]*

[a] Department of Textile Engineering, Yazd University, P.O. Box, 89195-741 Yazd, Iran.

[b] Department of Chemistry, Iran University of Science and Technology, P.O. Box, Narmak 16846-13114, Tehran, Iran

[1]These authors contributed equally to this work.

**Corresponding author:*

Mahdi Hasanzadeh, E-mail: m.hasanzadeh@yazd.ac.ir; Tel: +98-353-1232569; Fax: +98-353-8209817;

ORCID iD: 0000-0003-4951-8348

Table of content:

Figure S1. Chemical structure of organic dye (C.I. Acid Red 88).

Figure S2. The density of acidic and basic active sites on the surface of GO and GO/ZIF-8 nanocomposite.

Figure S3. The plots of isotherm models for adsorption of AR88 dye on the GO/ZIF-8 nanocomposite in (a) dark and (b) light conditions.

Figure S4. The plots of pseudo-first-order and pseudo-second-order kinetic models for adsorption of AR88 dye on the GO/ZIF-8 nanocomposite in (a) dark and (b) light conditions.

Figure S5. The plots of the intraparticle diffusion model for adsorption of AR88 dye on the GO/ZIF-8 nanocomposite in (a) dark and (b) light conditions.

Figure S6. Thermodynamic plot for the adsorption of AR88 dye on the GO/ZIF-8 nanocomposite.

Figure S7. Piezo-photocatalytic degradation rates of different dyes with GO/ZIF-8 nanocomposite.

Figure S8. The plots of kinetic of catalytic degradation of AR88 dye at different catalytic conditions of piezocatalytic, photocatalytic, and piezo-photocatalytic. (a-c) zero-order, (d-f) first-order, and (g-i) second order models.

Figure S9. Mass spectrum of AR88 dye after piezo-photocatalytic degradation**.**

Figure S10. Reusability test of the GO/ZIF-8 nanocomposite in piezo-photocatalytic degradation of AR88 dye.

Figure S11. XRD patterns of the GO/ZIF-8 nanocomposite before and after piezo-photocatalytic degradation of AR88 dye.

Table S1. The porous characteristics of the GO/ZIF-8 nanocomposite

Table S2. Detected intermediates of AR88 during piezo-photocatalytic degradation

Table S3. Comparison of the adsorption capacity of the GO/ZIF-8 nanocomposite with related adsorbents reported in the literature

Table S4. Comparison of the degradation performance of the GO/ZIF-8 nanocomposite with related catalysts reported in the literature

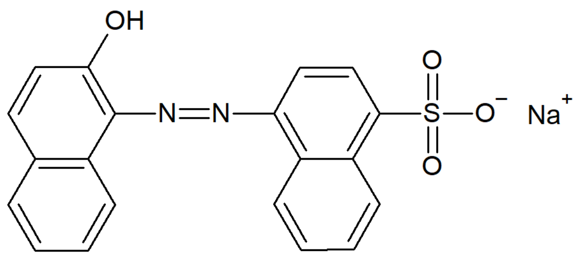

Figure S1. Chemical structure of organic dye (C.I. Acid Red 88).

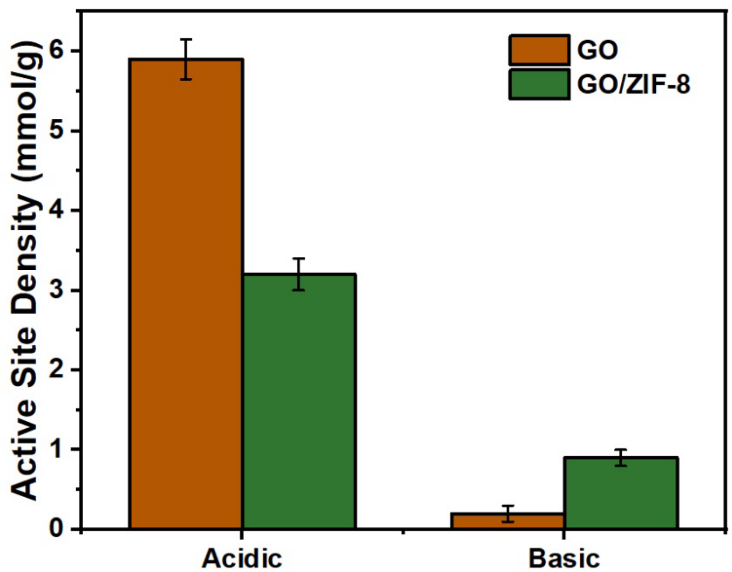

Figure S2. The density of acidic and basic active sites on the surface of GO and GO/ZIF-8 nanocomposite.

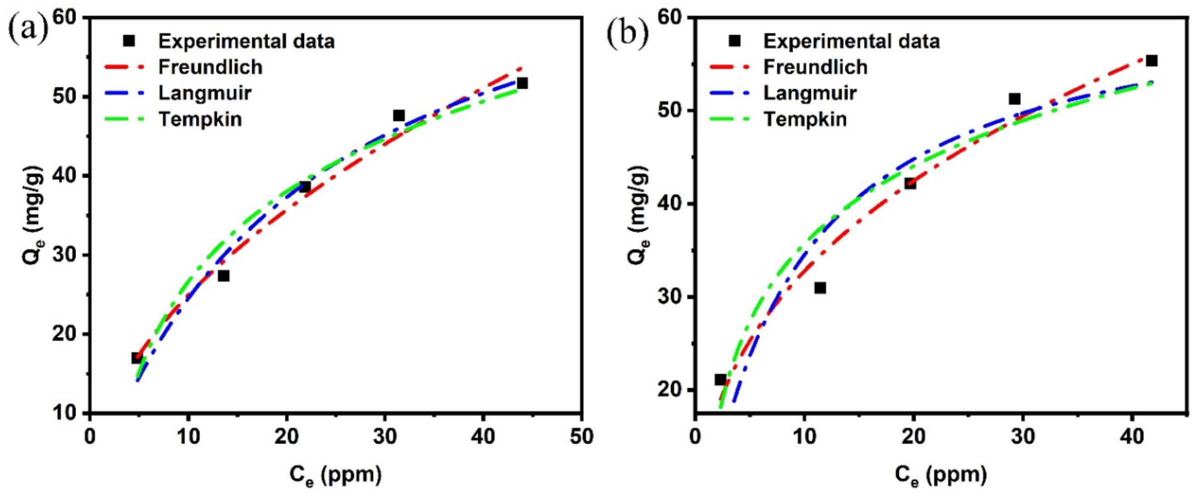

Figure S3. The plots of isotherm models for adsorption of AR88 dye on the GO/ZIF-8 nanocomposite in (a) dark and (b) light conditions.

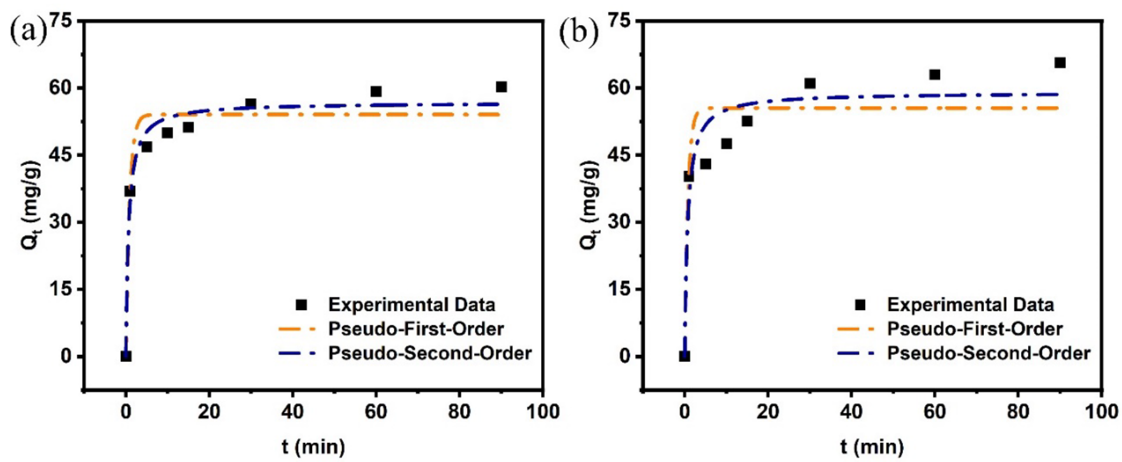

Figure S4. The plots of pseudo-first-order and pseudo-second-order kinetic models for adsorption of AR88 dye on the GO/ZIF-8 nanocomposite in (a) dark and (b) light conditions.

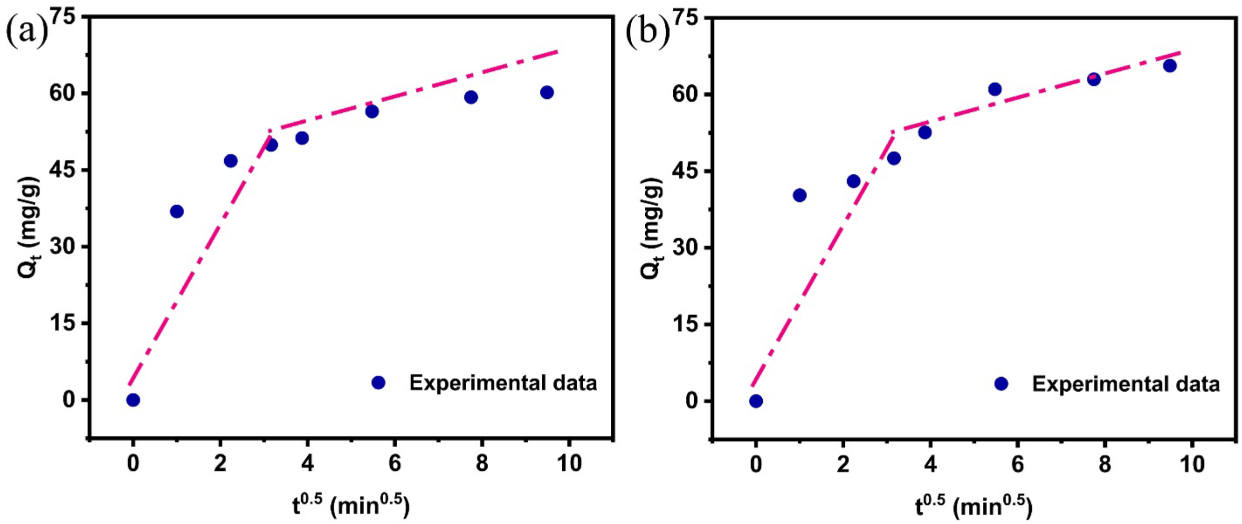

Figure S5. The plots of the intraparticle diffusion model for adsorption of AR88 dye on the GO/ZIF-8 nanocomposite in (a) dark and (b) light conditions.

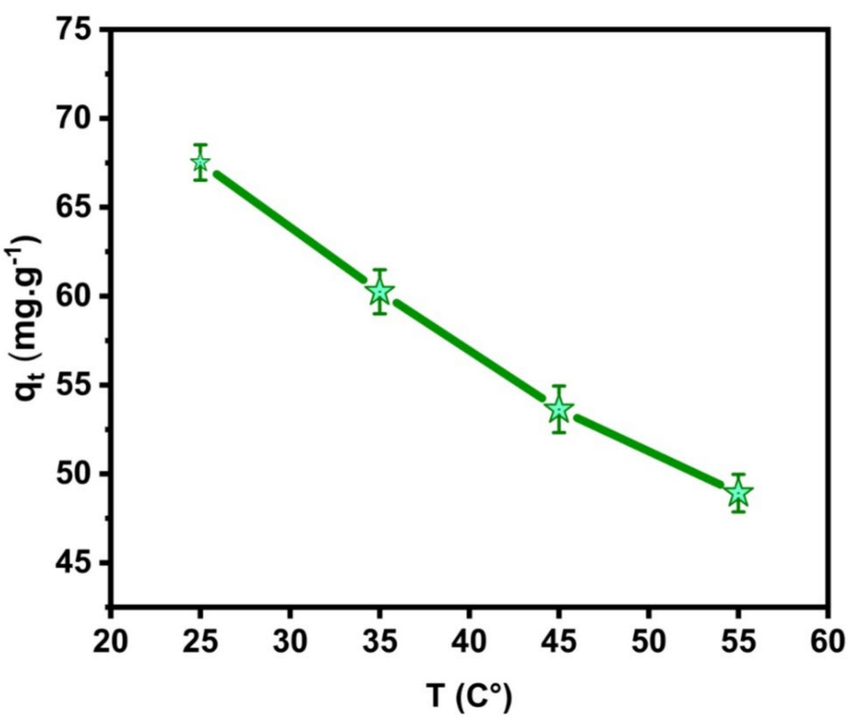

Figure S6. Thermodynamic plot for the adsorption of AR88 dye on the GO/ZIF-8 nanocomposite.

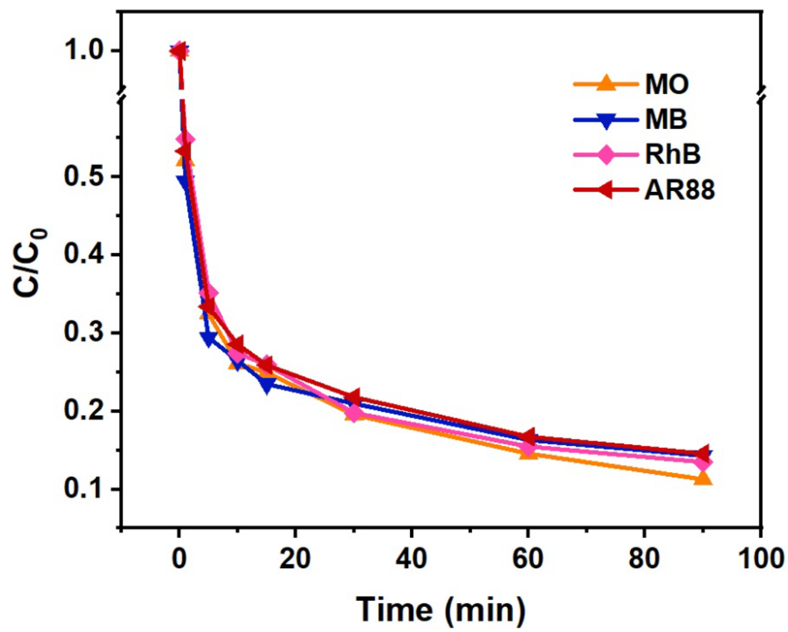

Figure S7. Piezo-photocatalytic degradation rates of different dyes with GO/ZIF-8 nanocomposite.

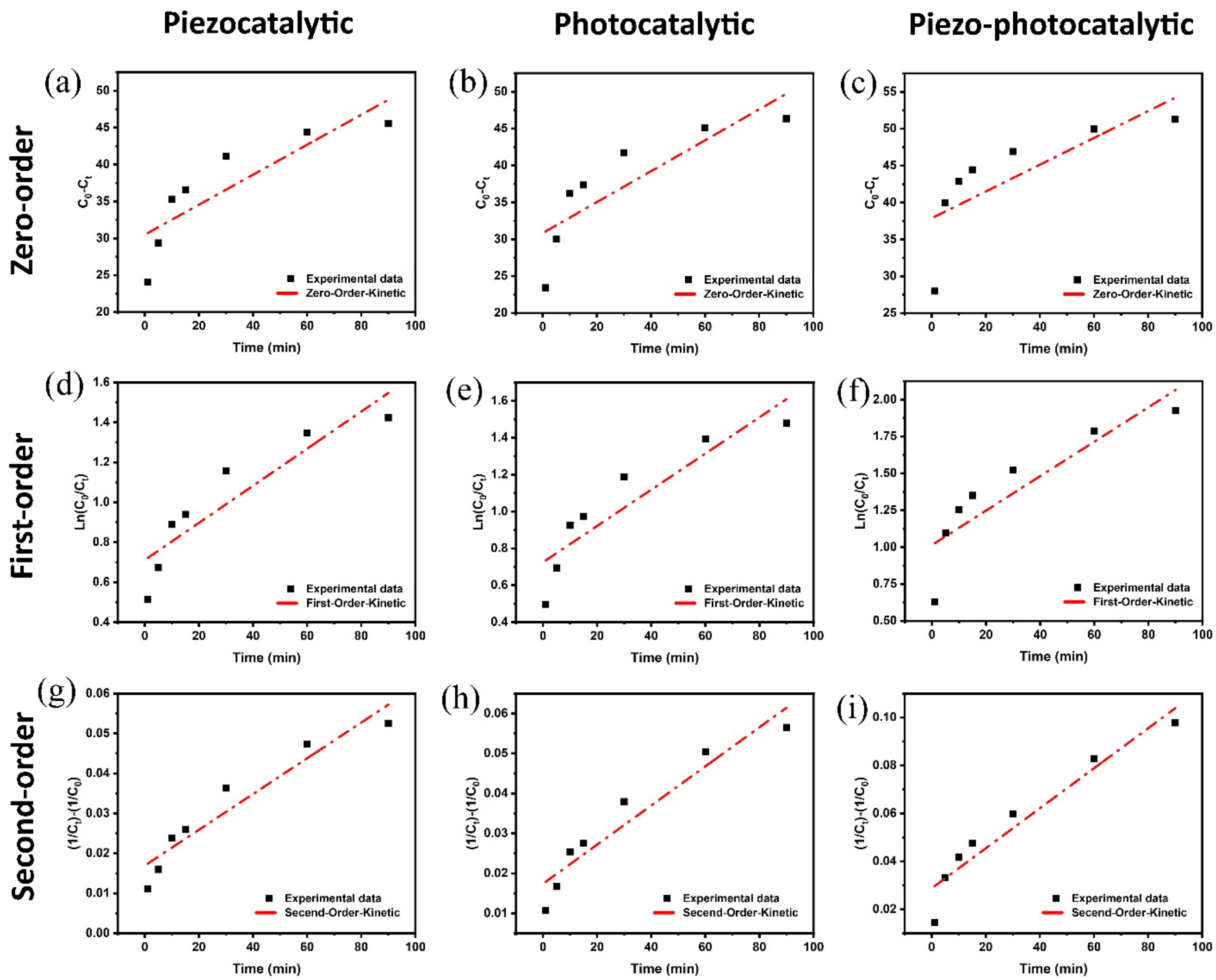

Figure S8. The plots of kinetic of catalytic degradation of AR88 dye at different catalytic conditions of piezocatalytic, photocatalytic, and piezo-photocatalytic. (a-c) zero-order, (d-f) first-order, and (g-i) second order models.

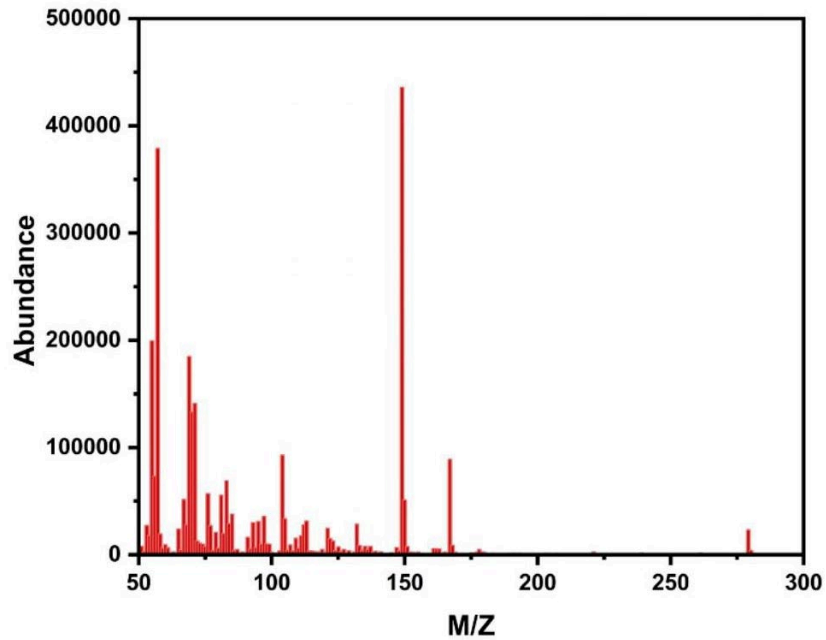

Figure S9. Mass spectrum of AR88 dye after piezo-photocatalytic degradation.

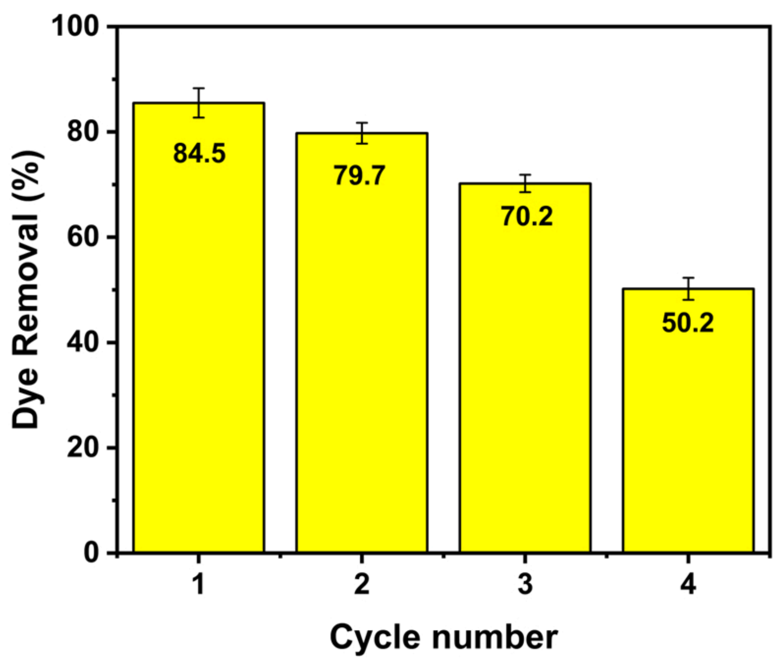

Figure S10. Reusability test of the GO/ZIF-8 nanocomposite in piezo-photocatalytic degradation of AR88 dye.

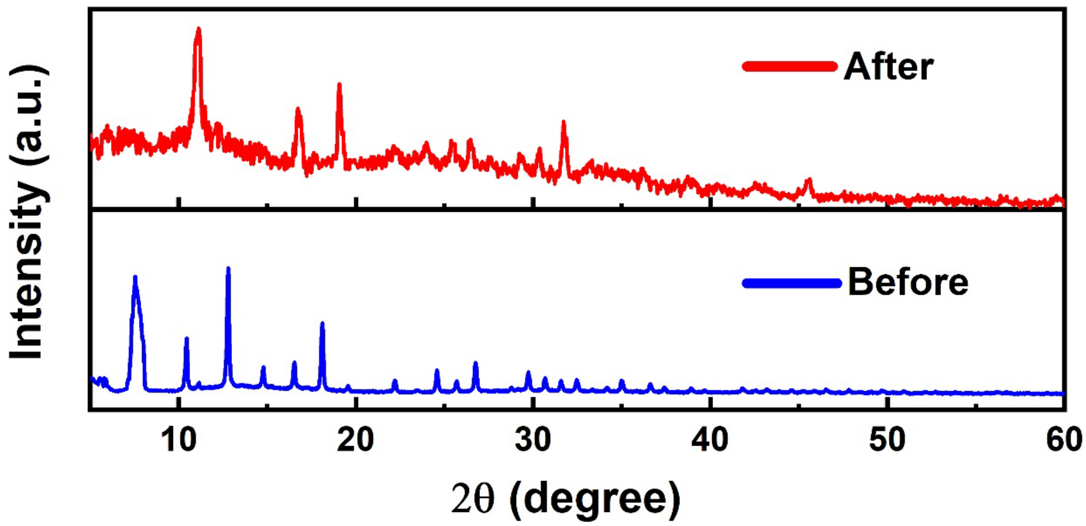

Figure S11. XRD patterns of the GO/ZIF-8 nanocomposite before and after piezo-photocatalytic degradation of AR88 dye.

Table S1. The porous characteristics of the GO/ZIF-8 nanocomposite

Sample	Specific surface area (m^2/g)	Pore volume (cm^3/g)	Pore width distribution (nm)
GO	85.27	0.031	2.45
ZIF-8	850.86	0.45	2.142
GO/ZIF-8	804.13	0.76	3.782

Table S2. Detected intermediates of AR88 during piezo-photocatalytic degradation

m/z	Proposed Compound	Suggested Structure Fragmentation	Chemical Structure
350	Acid Red 88 (AR88)	Parent dye molecule	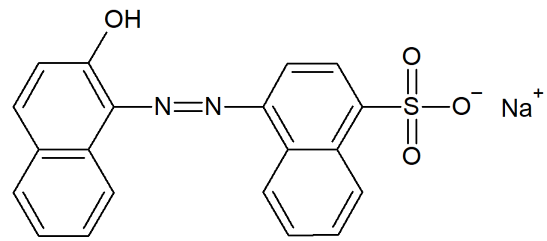
158	1,2-Naphthoquinone	Oxidized form of naphthalene-2-ol	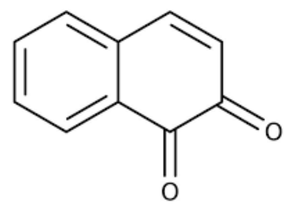
144	Naphthalene-2-ol / 1-amino-2-naphthol	Azo bond cleavage products	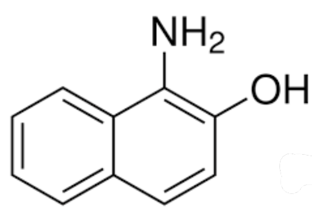
166	Phthalic acid	Oxidized ring-opening product	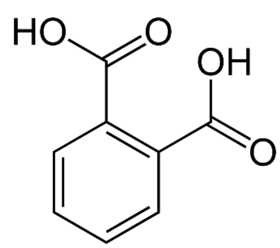
128	Naphthalene	Deaminated aromatic structure	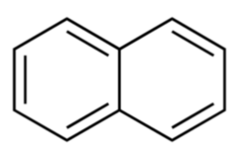

122	Benzoic acid	Terminal degradation product	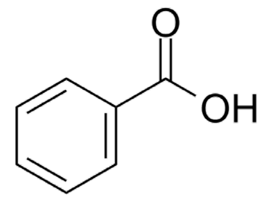
116	Maleic acid	Small chain dicarboxylic acid	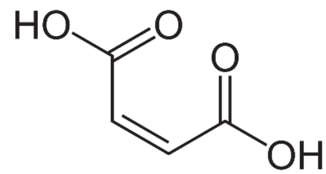

Table S3. Comparison of the adsorption capacity of the GO/ZIF-8 nanocomposite with related adsorbents reported in the literature

Adsorbent	Dye	Adsorption kinetic (isotherm)	Adsorption condition	Adsorption capacity (mg/g)	Ref.
Ag/ZnO/3DG	MB	PSO	m=0.3 mg, C_0=10 ppm	310	[1]
Fe_3O_4/GA	BPA	PSO (Langmuir)	m=20 mg, C_0=25-400 ppm	253.8	[2]
GO/1-octadecylamine	MG	PSO (Freundlich)	m=5 mg, C_0=50-2500 ppm	2687.56	[3]
PPGA	MO	PSO (Langmuir)	m=2.5 mg, C_0=1-70 ppm	202.8	[4]
GO/silk fibroin aerogels	MB	PSO (Langmuir)	m=1 mg, C_0=100 μmol/L	1322.71	[5]
rGO/TNT-3%	MB	PFO (Langmuir)	m=0.1 g, C_0=10-60 ppm	26.3	[6]
	MO			1.6	
Bi_2O_3@GO	RhB	PFO (Temkin /Langmuir)	m=5 mg, C_0=1-90 ppm	320	[7]
PFGA	MO	(Freundlich)	m=0.2 g, C_0=50-300 ppm	3059.2	[8]
	AM	(Langmuir)	m=0.2 g, C_0=50-300 ppm	2043.7	
3DG	MO	(Langmuir)	m=0.15 g, C_0=50-300 ppm, time = 60 min	27.93	[9]
GA	MB	PSO (Langmuir)	m=6 mg, C_0=20 ppm, time = 30 min	76	[10]
	MG			352	
	RhB			111	
	MO			16	
$CoFe_2O_4$/GO	MB	PSO (Langmuir)	m=30 mg, C_0=20 ppm, time = 7 h	355.9	[11]
	RhB			284.9	
	MO			53	

GO/ZIF-8	AR88	PSO (Freundlich)	m = 15 mg, C_0= 60 ppm	65.63	This study

3DG: three-dimensional graphene; GO: graphene oxide; PPGA: polydopamine and polyethylenimine co-functionalized graphene oxide aerogel; PFGA: polyethyleneimine-functionalized graphene aerogel; TNT: titanate nanotube; BPA: bisphenol A; AM; Amaranth; PFO: pseudo-first-order; PSO: pseudo-second-order.

Table S4. Comparison of the degradation performance of the GO/ZIF-8 nanocomposite with related catalysts reported in the literature

Photocatalyst	Dye	Catalytic condition	Degradation efficiency (%)	Ref.
Ag/ZnO/3DG	MB	m=0.3 mg, C_0=10 ppm	UV = 40 Visible = 43	[1]
rGO/TNT-3%	MB	m=0.1 mg, C_0=20 ppm, time = 60 min (UV) 180 min (visible)	UV = 100 Visible = 95	[6]
	MO	m=0.1 mg, C_0=20 ppm, time= 180 min	Visible = 99.1	
GO/ZIF-8	AR88	m = 15 mg, C_0= 60 ppm, time= 90 min	UV = 77.2 Ultrasonic= 75.9 UV + Ultrasonic= 85.4	This study

3DG: three-dimensional graphene; TNT: titanate nanotube.

References:

1. Kheirabadi M, Samadi M, Asadian E, Zhou Y, Dong C, Zhang J, Moshfegh AZ (2019) Well-designed Ag/ZnO/3D graphene structure for dye removal: Adsorption,

photocatalysis and physical separation capabilities. J Colloid Interface Sci 537:66–78

2. Quan LD, Dang NH, Tu TH, Phuong Linh VN, Mong Thy LT, Nam HM, Phong MT, Hieu NH (2019) Preparation of magnetic iron oxide/graphene aerogel nanocomposites for removal of bisphenol A from water. Synth Met 255:116106

3. Lv M, Yan L, Liu C, et al (2018) Non-covalent functionalized graphene oxide (GO) adsorbent with an organic gelator for co-adsorption of dye, endocrine-disruptor, pharmaceutical and metal ion. Chem Eng J 349:791–799

4. Xu J, Du P, Bi W, Yao G, Li S, Liu H (2020) Graphene oxide aerogels co-functionalized with polydopamine and polyethylenimine for the adsorption of anionic dyes and organic solvents. Chem Eng Res Des 154:192–202

5. Wang S, Ning H, Hu N, Huang K, Weng S, Wu X, Wu L, Liu J, Alamusi (2019) Preparation and characterization of graphene oxide/silk fibroin hybrid aerogel for dye and heavy metal adsorption. Compos Part B Eng 163:716–722

6. Nguyen CH, Juang RS (2019) Efficient removal of methylene blue dye by a hybrid adsorption–photocatalysis process using reduced graphene oxide/titanate nanotube composites for water reuse. J Ind Eng Chem 76:296–309

7. Das TR, Patra S, Madhuri R, Sharma PK (2018) Bismuth oxide decorated graphene oxide nanocomposites synthesized via sonochemical assisted hydrothermal method for adsorption of cationic organic dyes. J Colloid Interface Sci 509:82–93

8. Shu D, Feng F, Han H, Ma Z (2017) Prominent adsorption performance of amino-functionalized ultra-light graphene aerogel for methyl orange and amaranth. Chem Eng J

324:1–9

9. Labiadh L, Kamali AR (2019) 3D graphene nanoedges as efficient dye adsorbents with ultra-high thermal regeneration performance. Appl Surf Sci 490:383–394

10. Tang S, Xia D, Yao Y, Chen T, Sun J, Yin Y, Shen W, Peng Y (2019) Dye adsorption by self-recoverable, adjustable amphiphilic graphene aerogel. J Colloid Interface Sci 554:682–691

11. Chang S, Zhang Q, Lu Y, Wu S, Wang W (2020) High-efficiency and selective adsorption of organic pollutants by magnetic CoFe2O4/graphene oxide adsorbents: Experimental and molecular dynamics simulation study. Sep Purif Technol 238:116400